ISBN: 978-3-95450-227-1 ISSN: 2673-5490 doi:10.18429/JACoW-IPAC2022-MOPOMS023

# START-TO-END BEAM-DYNAMICS SIMULATIONS OF A COMPACT C-BAND ELECTRON BEAM SOURCE FOR HIGH SPECTRAL BRILLIANCE APPLICATIONS

L. Faillace, M. Behtouei, A. Giribono, B. Spataro, C. Vaccarezza, INFN-LNF, Frascati, Italy
L. Palumbo, F. Bosco, M. Carillo, L. Giuliano, M. Migliorati, A. Mostacci, Sapienza University of Rome Departement SBAI, Italy
J.B. Rosenzweig, O. Camacho, A. Fukasawa, N. Majernik, O. Williams, University of California, Los Angeles (UCLA) Department of Physics and Astronomy, USA
S. Tantawi, SLAC National Accelerator Laboratory, USA
R. Agustsson, D. Bruhwiler, I. Gadjev, S. Kutsaev, A. Murokh, RadiaBeam Technologies, USA

*Abstract*

Proposals for new linear accelerator-based facilities are flourishing world-wide with the aim of high spectral brilliance radiation sources. Most of these accelerators are based on electron beams, with a variety of applications in industry, research and medicine such as colliders, free-electron lasers, wake-field accelerators, coherent THz and inverse Compton scattering X/$\gamma$ sources as well as high-resolution diagnostics tools in biomedical science. In order to obtain high-quality electron beams in a small footprint, we present the optimization design of a C-band linear accelerator machine. Driven by a novel compact C-band hybrid photoinjector, it will yield ultra-short electron bunches of few 100's pC directly from injection with ultra-low emittance, fraction of mm-mrad, and a few hundred fs length simultaneously, therefore satisfying full 6D emittance compensation. The normal-conducting linacs are based on a novel high-efficiency design with gradients up to 50 MV/m. The beam maximum energy can be easily adjusted in the mid-GeV's range. In this paper, we discuss the start-to-end beam-dynamics simulations in details.

## INTRODUCTION

Electron beams with high peak currents and ultra-low normalized emittances, therefore ultra-bright, are essential for the new linear accelerator-based facilities promising numerous applications, such as electron-positron or photon-photon colliders [1,2], X-ray free-electron lasers [3,4], wakefield accelerator experimentation, coherent THz and inverse Compton scattering X-ray or γ-ray sources [5]. Other applications reside in the field of biomedical science, where low emittance photon beams are used to obtain high quality images for diagnostics due to the increased resolution and contrast they can provide [6, 7]. In order to obtain high brightness electron beams, photoinjectors [8-10], in which electron bunches are generated from the cathode metallic surface by illumination via a femtosecond-to-picosecond laser, have been the essential instrument in worldwide use for that last three decades.

## RF DESIGN OF THE HYBRID PHOTOINJECTOR

The proposed *hybrid* RF photoinjector is composed of a photocathode embedded in an initial 2.5 gun cell standing-wave (SW) section connected through an input coupling cell directly to a traveling-wave (TW) section (see Fig. 1).

The are several advantages of this hybrid system compared with conventional split SW/TW injectors:

- Cancellation of RF reflections from the SW section (no circulator needed);
- Bunch lengthening effect, due to the ballistic drift, is reduced (the cell that couples the two structures replaces the long beam pipe and matching-section following the RF gun);
- The RF coupling between the SW and the TW sections optimally results in a 90 deg phase shift of the accelerating field → *strong velocity bunching* effect applied to the beam;
- Production of very short bunch lengths, over an order of magnitude smaller.

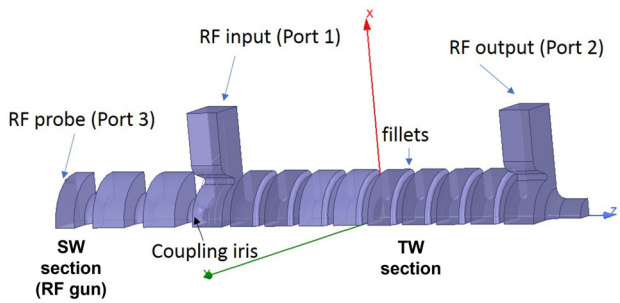


Figure 1: electromagnetic model of the gun.

The RF design was performed with the Ansys 3D code [11]. The main RF parameters are given in Table 1, and previously reported in [12-14]. The required rf input power is about 40 MW in order to obtain a peak surface electric field at the cathode equal to 120 MV/m. The ratio between the SW on-axis peak electric field and the average TW electric field is equal to $E_{z,p,SW}$ /⟨$E_{z,TW}$ ⟩ = 3.25, where

ISBN: 978-3-95450-227-1 ISSN: 2673-5490 doi:10.18429/JACoW-IPAC2022-MOPOMS023



$E_{z,p,SW}$ is also the maximum field value $E_{max}$ of the on-axis accelerating electric field.

In order to improve the power efficiency of the hybrid photoinjector, we have also investigated a tapered TW section and it was possible to reduce rf input power to about 20 MW versus the 40 MW required for the original design.

Table 1: Main Parameters of the C-band Photoinjector

| RF Parameter | SW | TW |
|---|---|---|
| Operation mode | π | 2π/3 |
| Quality factor, $Q$ | 9,900 | 9,900 |
| Eff. shunt impedance, $R_{sh}$ | 52 MΩ/m | 65 MΩ/m |
| Mode separation | 21.5 MHz | 40 MHz |
| Build-up time, $\tau$ | 530 ns | - |
| Group velocity, $v_g$ | - | 2.73 % |
| Attenuation, $\alpha$ | - | 0.23 $m^{-1}$ |
| Filling time, $T_f$ | - | 21.3 ns |

The on-axis electric field amplitude profile and phase distribution are shown in Figs. 2 and 3, respectively. The π/2 phase-shift between the SW and TW section, a particular feature of this hybrid structure, allows for velocity bunching thus obtaining ultra-short beams.

The photoinjector prototype has been recently fabricated and tested with high RF power. The preliminary beam measurements have also been carried out, showing good agreement with simulations. Results will be published in a forthcoming paper.

## BEAM DYNAMICS SIMULATIONS

The start-to-end simulations were carried out with the GPT code [15] and details are found in [16]. The beam input parameters are listed in Table 2. The beam exit energy is about 4 MeV. Two energy scenarios are investigated:

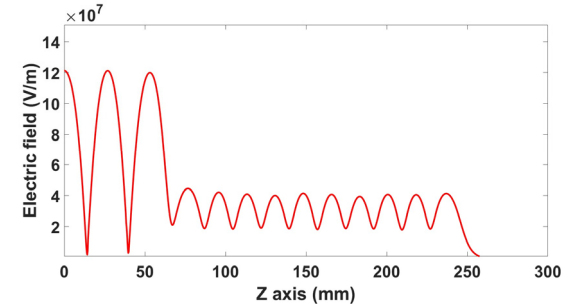


Figure 2: On-axis electric field amplitude profile.

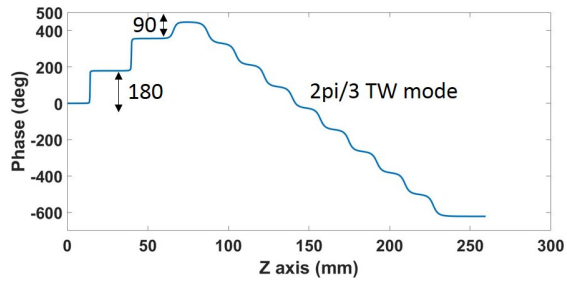


Figure 3: On-axis electric field phase distribution.

medium-energy (220 MeV) for the Compton source and high-energy (400 MeV) for the FEL scenario, in which case the photoinjector is followed by eight high-gradient Tantawi-style C-band linacs at 50 MV/m [17].

All parameters were optimized in order to obtain beam emittance minimization, to $\epsilon_n$ = 0.5 mm-mrad. This condition is reached simultaneously with bunch compression down to $\sigma_z$ = 200 fs.

More in-depth beam slice analysis and wakefields/beam break-up studies can be found in [18, 19].

## COMPTON AND FEL APPLICATIONS

In Fig. 4 are shown the RMS beam sizes $\sigma_x$ and $\sigma_y$ in the inverse Compton scattering (ICS) system operated at 220 MeV, from GPT start-to end simulation. The focal

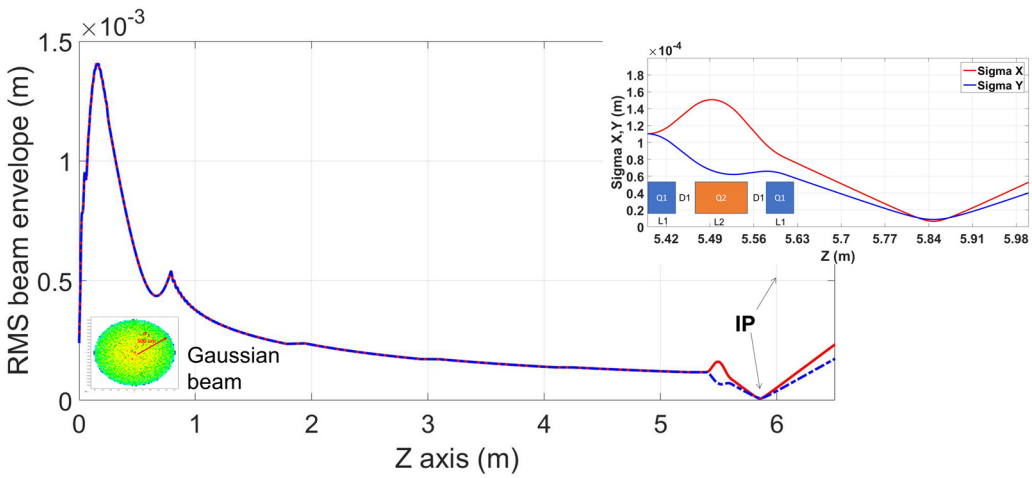


Figure 4: RMS beam sizes $\sigma_x$ and $\sigma_y$ in the ICS system operated at 220 MeV, from GPT start-to end simulation.

ISBN: 978-3-95450-227-1 ISSN: 2673-5490 doi:10.18429/JACoW-IPAC2022-MOPOMS023

system is composed of a tunable permanent magnet triplet array with lengths of 6 cm - 12 cm - 6 cm and nominal gradients of 102 T/m - 94 T/m - 102 T/m, respectively. The interaction region which illustrates the predicted very compact (below 9 μm) spot sizes.

Table 2: Beam Dynamics Simulations Beam Input Parameters

| Parameter | Value |
|---|---|
| Beam Charge, Q | 250 pC |
| Spot sizes, $\sigma_{x,y}$ (cut@1$\sigma$) | 500 μm |
| Laser Pulse Length | 0.5 ps |
| E-field at cathode | 120 MV/m |
| # particles | 50,000 |

Due to the considerable longitudinal compression the hybrid design imparts, the corresponding high peak current is beneficial for an x-ray FEL, in terms of the gain length and photon-per-pulse output. Linear transformations matching the transverse phase-space orientation were performed to optimize the gain through an 8 m FD lattice with 15 T/m quadrupoles in GENESIS. These optimal matching dimensions, along with other relevant simulation parameters, are reported below in Table 3. The GENESIS simulation results, as shown in Fig. 5, indicate saturation and lasing at λ = 6.0 nm, with a mean single shot energy output of 62 μJ.

Table 3: FEL Simulations Input Parameters

| Parameter | Value |
|---|---|
| Beam Charge, $Q$ | 250 pC |
| Spot Dimensions, $\sigma_{x,y}$ | 22x15 $\mu m$ |
| Normalized Emittance, $\varepsilon_{n,r}$ | 0.5 mm-mrad |
| Bunch Length, $\sigma_z$ | 190 fs |
| Mean Energy, $\gamma mc^2$ | 400 MeV |
| Fractional Energy Spread | 0.054 % |

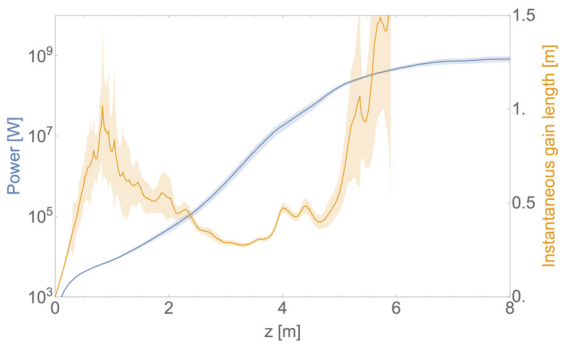


Figure 5: Instantaneous gain length (orange) and laser power(blue) as calculated in GENESIS. The peak power at saturation is approximately 830 MW.

Moreover, by adding two more linac sections (thus increasing to the final energy and permitting off-crest operation in part of the linac) and a compact (~1 m) chicane, we can enable a soft x-ray FEL operating in the water window at λ = 4 nm. The increased current has a dramatic effect on the peak power (4.2 GW is predicted).

## CONCLUSIONS

We have presented a new class of a compact hybrid (SW/TW) photoinjector, operating in C-band at 5.712 GHz with an electric field of 120 MV/m at the cathode. Such an electron source is meant for next generation linac accelerator-based research facilities.

The RF design and beam dynamics analysis have been performed in order to obtain a full 6D emittance compensation (both on the transverse and longitudinal planes) with a 250 pC electron bunch. There is a large number of advanced scenarios for the application of the compact C-band hybrid photoinjector, e.g. wakefield accelerators, THz sources and applications requiring a compact mobile source. We have simulated two applications: examination as the injector of an intermediate-energy (220 MeV) ICS monochromatic gamma-ray source, which takes advantage of the beam focusability and its short pulse length. Indeed, we have studied a working point which utilizes a beam spot size less than 10 μm at the interaction point located at less than 6 m from the cathode; investigation of a higher energy (400 MeV) soft X-ray FEL. Again with a modest footprint, we demonstrated the possibility of lasing at 4 nm, producing a compact water-window free-electron laser in 10 m length. For completeness we note that the utility of the hybrid injector in application is validated by studies of beam stability and alignment tolerances, issues which are more challenging in this very high-performance system.

## ACKNOWLEDGEMENTS

This work is partially supported by DARPA under the Contract No. HR001120C0072, by DOE Contract DE-SC0009914, DOE Contract DE-SC0020409, and by the National Science Foundation Grant No. PHY-1549132.

## REFERENCES

[1] V. Shiltsev and F. Zimmermann, "Modern and future colliders", *Rev. Mod. Phys*. vol. 93, p. 015006, 2021.

[2] L. Schoeffel, C. Baldenegro, H. Hamdaoui, S. Hassani, C. Royon, and M. Saimpert, "Photon–photon physics at the LHC and laser beam experiments, present and future", *Prog. Part. Nucl. Phys*., p. 103889, 2021.

[3] J. Rosenzweig *et al.*, "An ultra-compact X-ray free electron laser", *New J. Phys.* vol. 22, p. 093067, 2020.

[4] M. Ferrario *et al.*, "EuPRAXIA@SPARC_LAB Design study towards a compact FEL facility at LNF", arXiv:1801.08717.

[5] L. Faillace *et al.*, "Status of compact inverse compton sources in Italy:BriXS and STAR, Advances in Laboratory-

ISBN: 978-3-95450-227-1 ISSN: 2673-5490 doi:10.18429/JACoW-IPAC2022-MOPOMS023



based X-Ray Sources, *Optics, and Applications VII,* vol. 11110, International Society for Optics and Photonics, p. 1111005, 2019.

[6] L. Rigon, "2.08 - X-ray imaging with coherent sources", *Comprehensive Biomedical Physics* edited by A. Brahme, Elsevier, Oxford, pp. 193–220, 2014.

[7] W. Graves, "High brilliance x-rays from Compact Sources", in *Proc. High Brightness Electron Beams Workshop*, San Juan, Puerto Rico, 2013, http://pbpl.physics.ucla.edu/HBEB2013/Talks/WilliamGravesHBEB13.pptx

[8] B. Carlsten, "New photoelectric injector design for the Los Alamos National Laboratory XUV FEL Accelerator", *Nucl. Instrum. Methods Phys. Res., Sect. A* vol. 285, p.313 881, 1989.

[9] F. Zhou e*t al.*, "Commissioning of the SLAC linac coherent light source II electron source", *Phys. Rev*. vol. 887 Accel. Beams 24, p. 073401, 2021.

[10] R. R. Robles, O. Camacho, A. Fukasawa, N. Majernik, and J. B. Rosenzweig, "Versatile, high brightness, cryogenic photoinjector electron source", *Phys. Rev. Accel. Beams* vol. 24, p. 891 063401, 2021.

[11] https://www.ansys.com/products/electronics/ansys-hfss

[12] L. Faillace *et al.,* "Beam Dynamics for a High Field C-Band Hybrid Photoinjector", in *Proc. IPAC'21*, Campinas, Brazil, May 2021, pp. 2714-2717. doi:10.18429/JACoW-IPAC2021-WEPAB051

[13] M. Carillo *et al.*, "Three-Dimensional Space Charge Oscillations in a Hybrid Photoinjector", in *Proc. IPAC'21*, Campinas, Brazil, May 2021, pp. 3240-3243. doi:10.18429/JACoW-IPAC2021-WEPAB256

[14] F. Bosco *et al.*, "Modeling Short Range Wakefield Effects in a High Gradient Linac", in *Proc. IPAC'21*, Campinas, Brazil, May 2021, pp. 3185-3188. doi:10.18429/JACoW-IPAC2021-WEPAB238

[15] http://www.pulsar.nl/gpt/index.html

[16] L. Faillace *et al*., "High field hybrid photoinjector electron source for advanced light source applications", *Phys. Rev. Accel. Beams* vol. 25, p. 063401, Jun. 2022.

[17] S. Tantawi *et al*., "Design and demonstration of a distributed-coupling linear accelerator structure", *Phys. Rev. Accel. Beams* vol. 23, p. 092001, 2020.

[18] M. Carillo *et al.*, "Space Charge Analysis for Low Energy Photoinjector", presented at the IPAC'22, Bangkok, Thailand, Jun. 2022, paper WEPOMS017, this proceedings.

[19] F. Bosco *et al.*, "Modeling and Mitigation of Long-Range Wakefields for Advanced Linear Colliders", presented at the IPAC'22, Bangkok, Thailand, Jun. 2022, paper WEPOMS045, this proceedings.

[19] http://genesis.web.psi.ch/index.html